Acta Cryst B
STRUCTURAL SCIENCE
CRYSTAL ENGINEERING
MATERIALS

ISSN 2052-5206

Preliminary observations of the interplay of radiation damage with spin crossover

Dmitry Chernyshov,[a]* Vadim Dyadkin[a] and Karl Wilhelm Törnroos[b]

[a]Swiss–Norwegian BeamLines at the European Synchrotron Radiation Facility, 38000 Grenoble, France, and [b]Department of Chemistry, University of Bergen, Allégaten 41, 5007 Bergen, Norway. *Correspondence e-mail: dmitry.chernyshov@esrf.fr

Received 22 November 2021
Accepted 2 May 2022

Edited by S. Grabowsky, University of Bern, Switzerland

Keywords: radiation damage; synchrotron radiation; spin crossover compound.

CCDC references: 2169944; 2169945; 2169946

Supporting information: this article has supporting information at journals.iucr.org/b

Intense synchrotron radiation makes time-resolved structural experiments with increasingly finer time sampling possible. On the other hand, radiation heating, radiation-induced volume change and structural disorder become more frequent. Temperature, volume change and disorder are known to be coupled with equilibrium in molecular spin complexes, balancing between two or more spin state configurations. Combining single-crystal diffraction and synchrotron radiation it is illustrated how the radiation damage and associated effects can affect the spin crossover process and may serve as yet another tool to further manipulate the spin crossover properties.

1. Introduction

Some octahedral complexes of 3d block transition metals can be found in a few stable electronic states. Thus, for Fe^{2+} the Low Spin (LS) configuration is less degenerate than the High Spin (HS) state and the entropy difference makes the HS states energetically favourable if the temperature is sufficiently high (Nicolazzi & Bousseksou, 2018).

The change of the spin state can alter colour, magnetization, density, crystal and molecular structures; this is why spin crossover materials are considered to be useful for many applications, ranging from medicine to electronics (Murray, 2013). Spin crossover phenomena are also of fundamental interest as they deal with complex spatio-temporal responses of interacting molecular complexes to external perturbations. The structure and properties of an individual spin-active molecule can be well understood through quantum chemistry, providing that intermolecular interactions are reduced to a mean-field (Paulsen *et al.*, 2013). The interactions between molecular units may be modelled with mechanistic toy models based on Ising-like Hamiltonians [electro-lattice models, *e.g.* Ndiaye *et al.* (2021)], as by its very nature this approach neglects many intra-molecular degrees of freedom. For any real spin crossover material however, change of properties associated with the change of spin states can neither be reduced to a behaviour of an isolated individual molecule nor simplified to mechanistic models; this is why, together with theoretical modelling, the structural experiment remains the most important source of information on the microscopic processes comprising spin crossover phenomena (Pillet, 2021).

Synchrotron radiation offers unique tools to characterize spin crossover, in particular fast diffraction probes of the crystal structure as a function of temperature, pressure, laser irradiation and any other external perturbation that may change the spin state (Collet & Guionneau, 2018). Switching

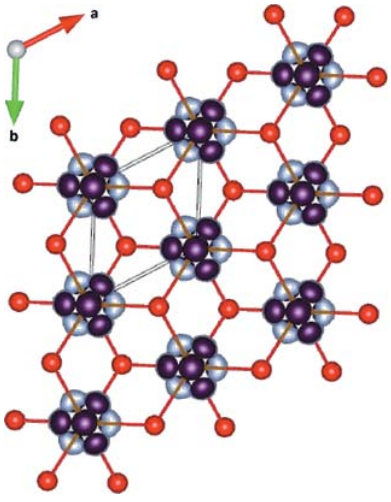

Table 1
Crystal data and structure refinement at 257 K.

Empirical formula	$C_{11}H_{34}Br_2FeN_6O$
Formula weight	482.11
Temperature	257 (2)
Wavelength (Å)	0.78405
Crystal system, space group	Trigonal, $R\bar{3}m$: H
Unit-cell dimensions, a (=b), c, γ (Å, °)	7.3806 (2), 31.5783 (16), 120
Volume (Å^3)	1489.71 (2)
Z, calculated density (Mg m^{-3})	4, 1.612
Absorption coefficient (mm^{-1})	6.110
F(000)	738
Crystal size (mm)	0.16 × 0.220 × 0.240
Theta range (°) for data collection	2.134–29.331
No. of reflections collected, unique, R_{int}	2292, 393, 0.0074
Completeness to θ = 28.062°	94.8
Refinement method	Full-matrix least-squares on F^2
No. of data, restraints, parameters	397, 1, 33
Goodness-of-fit on F^2	1.234
Final R indices [$I > 2\sigma(I)$]	$R1$ = 0.0379, $wR2$ = 0.1074
R indices (all data)	$R1$ = 0.0381, $wR2$ = 0.1076
Largest difference peak and hole (e Å^{-3})	0.437, −0.582

of the spin state by high-energy X-ray radiation (synchrotron) is also reported (Vankó *et al.*, 2007). However, synchrotron radiation interacts with matter in a complex way (Bras *et al.*, 2021). Radiation heating (Lawrence Bright *et al.*, 2021), radiation damage (Bogdanov *et al.*, 2021), radiation-induced volume change (Coates *et al.*, 2021) and structural disorder (Christensen *et al.*, 2019) exemplify some of the radiation-induced phenomena commonly observed. With temperature, volume change, and disorder known to be linked to the spin equilibrium; thus far we are not aware of any reports on radiation damage as a mechanism to influence the spin states in spin crossover materials. Here we present, as a first step, a spin crossover scenario for radiation-damaged $[Fe^{2+}(tame)_2]Br_2$·MeOH [tame = 1,1,1-tris(aminomethyl)ethane], derived from a multi-temperature (60 data sets) single-crystal synchrotron diffraction experiment and the ensuing sequential structure refinement.

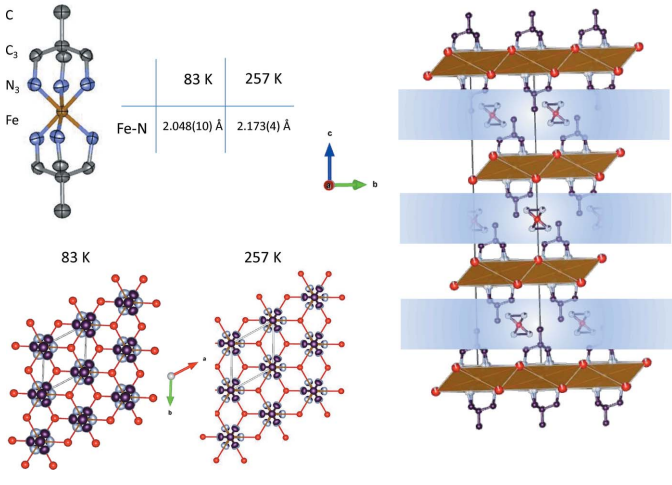

Figure 1
Top left: molecular structure of the spin-active cation $[Fe(tame)_2]^{2+}$ and Fe—N bond distances characteristic for HS (257 K) and LS (83 K) states, hydrogen atoms are omitted for clarity. Right: ionic layers of $[Fe(tame)_2]^{2+}$ cations and Br^- anions separated by van der Waals layers of ligands and disordered solvent. Bottom left: ionic layers with Br^- anions (red) and spin-active molecules, with ADPs at the 80% level, at the end (83 K) and at the beginning (257 K).

2. Experiment

Data were collected at the BM01 end station of the Swiss-Norwegian Beamlines, at the ESRF (Grenoble, France), with the Pilatus@SNBL diffractometer (Dyadkin *et al.*, 2016). The temperature was controlled with a Cryostream 700+, with diffraction data measured every 3 K on cooling in a range of 260–83 K with λ = 0.78405 Å (15.8 keV) with a single axis full rotation and one second per one degree sampling. The temperature range was expected to cover the full spin state change, from nearly pure HS to nearly pure LS state, based on a previous report for Cl-based analogue (Bernhardt *et al.*, 2018). The data were processed sequentially with *CrysAlis Pro* software (Rigaku, 2015), the initial structural model was derived with *SHELXT* (Sheldrick, 2015*a*) and then refined with *SHELXL* (Sheldrick, 2015*b*) in a sequential manner, as described by Chernyshov *et al.* (2019) and Bogdanov *et al.* (2021). Representative parameters characterizing the data at 257 (2) K and refinement are given in the Table 1.

The crystal structure is found to be disordered, for both the MeOH solvent molecule and also for the spin-crossover unit.

As shown by previous DFT calculations (Bernhardt *et al.*, 2018), the $[Fe(tame)_2]^{2+}$ cation is stabilized by a torsional libration of the each tripodal claw about its *C*3 axis onto either side of the vertical glide plane hosting an aminomethylene arm. The disorder is fixed by symmetry and we observe neither additional Bragg reflections nor diffuse scattering indicating long- or short-range ordering of the spin-active cations. The crystal structure is layered, with layers of the $[Fe(tame)_2]^{2+}$ cations and the Br^- anions separated by layers of the disordered MeOH solvent molecules; all the layers are orthogonal to the threefold *c*-axis, isomorphous to the Cl analogue (Bernhardt *et al.*, 2018), see Fig. 1 (left). One more sign of disorder is the apparent C—N distances (1.45 Å at 275 K) that are lower than expected 1.49 Å and abnormally decrease on cooling (1.41 Å at 83 K) together with ADPs. The quality of

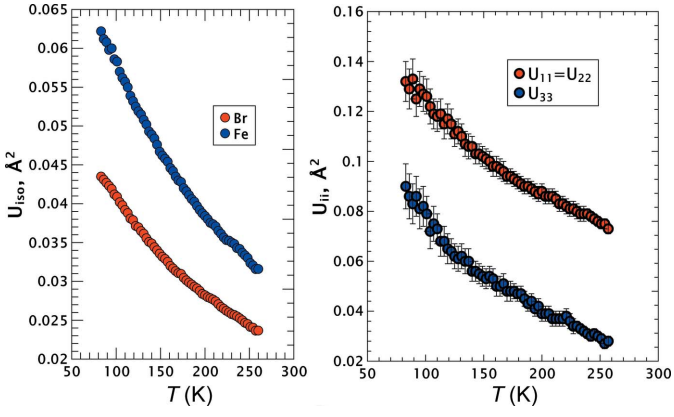

Figure 2
(Left) Isotropic displacement parameters for Fe and Br atoms. (Right) ADPs from C1 (top and bottom terminal atoms of the spin crossover cation, see Fig. 1).

refinement was progressively degraded on cooling together with an increase of the anisotropic displacement parameters (ADPs) for all atoms (Figs. 1 and 2). However, R_{int} values were practically the same for the all data sets. R_{int} is normally examined during *in situ* synchrotron experimentation to characterize the data quality, we see that monitoring of this descriptor only is not sufficient to detect radiation damage effects.

3. Results

3.1. Unit-cell dimensions

The isomorphous $[Fe^{2+}(tame)_2]Cl_2{\cdot}MeOH$ (Bernhardt *et al.*, 2018) shows an expected volume contraction upon cooling with spin conversion towards the LS state. In accordance with the layered structure the contraction is mostly seen along the *c*-axis, while the *a*-axis is practically invariant. Conversely, the Br analogue, studied here subject to radiation damage, shows a very different behaviour (Fig. 3). The volume thermal contraction changes to an expansion at ≈ 160 K and at 80 K we observe a unit-cell volume similar to that at 250 K. Note that the dose of absorbed radiation was accumulated upon cooling and that the volume expansion can therefore be related to radiation damage, similar to what was observed previously (Coates *et al.*, 2021).

Unit-cell dimensions however behave anisotropically, the more rigid intra-layer *a*-direction stays nearly constant down to 200 K and then expands at lower temperatures. The inter-layer *c*-direction contracts down to 150 K and then slowly increases. Such a behaviour suggests that the radiation damage induces some atomic displacements, firstly along the layer planes and then normal to layer direction.

3.2. Bonds and spin states

Conversion from LS to HS leads to an elongation of the Fe—N bonds by ≈ 0.15 Å. For the average structure, the Fe—N bonds change their length with temperature as a function of spin state. The temperature dependence of the Fe—N bonds therefore characterizes a transition scenario. A crossover between HS and LS states was observed for the Cl analogue with Fe—N bonds changing from 2.035 Å (LS) to 2.189 Å (HS) (Bernhardt *et al.*, 2018). An overlay of previously reported data with those for $[Fe^{2+}(tame)_2]Br_2{\cdot}MeOH$ shows a very different behaviour for the latter, suffering from radiation damage (Fig. 4). We assume that radiation damage slows down the spin conversion. One may expect that the temperature of the spin state equilibrium, $T1_{1/2}$, is higher for the Br-based compound in comparison with the Cl analogue. Such a trend is also reported for other SCO materials (Kuroda-Sowa *et al.*, 2017; Lemercier *et al.*, 2006). The scenario observed here may therefore be seen as a radiation-induced crossover between two transition curves as schematically shown in Fig. 4.

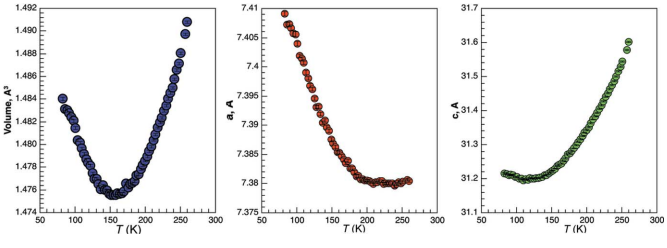

Figure 3
Volume and unit-cell dimensions as functions of temperature. (Left) unit-cell volume (Å^3). (Center) *a*-axis (Å). (Right) *c*-axis (Å).

4. Conclusion

The present finding are preliminary observations of a truly interesting phenomenon that needs further work to be properly understood, rationalized, and controlled.

The wavelength (0.7805 Å), of the synchrotron radiation was relatively close to the Br absorption edge (0.9202 Å), and the data collected upon cooling show the effect of the radiation dose accumulated progressively with time and temperature. The radiation damage manifests itself in the anisotropic expansion of the unit cell with a dose increase that over-compensates the expected temperature and spin-state related thermal contraction. An increase of the ADPs for all atoms with dose on cooling also serves as an indication of the disorder induced by the radiation, in agreement with the previous reports (Christensen *et al.*, 2019).

We observed that the radiation damage slows down the spin conversion and a final LS state is reached at lower temperatures than expected. This effect may tentatively be attributed to the volume effects which were previously seen with an applied pressure (Gütlich *et al.*, 2005). Indeed, application of a pressure normally favours formation of the LS states with its shorter Fe—N bonds shifting the transition curve to higher temperatures. It follows from Fig. 4 that the radiation-induced increase of the unit-cell volume might therefore favour HS extended states shifting the transition curve to lower temperatures.

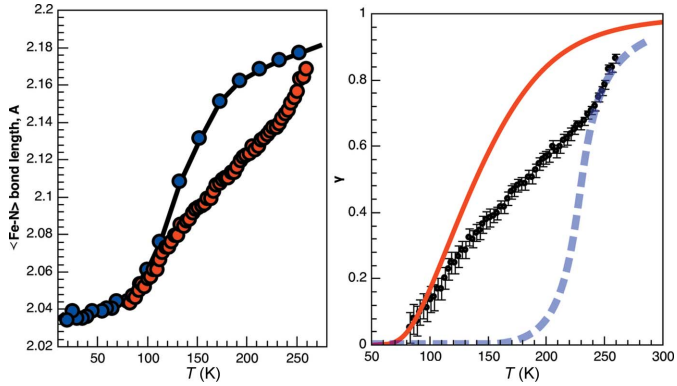

Figure 4
(Left) Fe—N bond distance as a function of temperature for the Cl (blue) and Br (red) analogues. (Right) HS fraction as a function of temperature, points with error bars are calculated from the bond lengths, the solid line represents a model curve derived by Bernhardt *et al.* (2018), the dashed curve shows a possible transition scenario for the Br analogue without radiation damage.

There still are many questions to be answered in future experimental studies. A precise control of the absorbed dose and a dose rate on the spin conversion has to be studied, either via measurement of the transmission or using estimates similar to the reported recently (Christensen *et al.*, 2019). The increase of the ADPs with the absorbed dose may be used as an internal structural measure of the degree of damage. It would be necessary to combine the dose accumulation at the energy close to an absorption edge with the data collection at lower or much higher energies of the X-ray radiation; such a scheme allows for the study of the crystal structure with temperature for a given dose and to avoid accumulation of the radiation damage during the data acquisition. The light-induced spin state trapping (LIESST) and relaxation processes in radiation-damaged samples also need to be probed; the interplay of radiation-induced disorder with generation, growth and decay of photo-excited spin states thus still remain to be uncovered.

A link between spin state switching and radiation-induced disorder can be mapped with a help of Ising-like model for spin crossover with structural disorder (Chernyshov *et al.*, 2007). This approach assumes that radiation-induced disorder merely shifts energy levels for HS and LS states, and the energy levels become dose dependent, see *Appendix A* for details.

All together these findings show that it is possible to have a low temperature LS state with the volume as large as for the virgin HT, HS state, and possibly record different transition scenarios for the same material but with different degrees of the radiation damage. The radiation damage can therefore play a constructive role as a tuning parameter for the premeditated control of SCO properties.

APPENDIX *A*
Phenomenological consideration of the radiation damage and spin equilibrium.

With an Ising-like model of spin crossover, the interactions between spin active molecules are given by the following Hamiltonian:

$$H_0 = \Delta \sum \sigma_i + \sum J_{ij}\sigma_i\sigma_j, \tag{1}$$

where σ_i is a pseudo spin (+1 for HS and −1 for LS state at the node i), Δ is the free energy difference between two states, and J_{ij} is an effective interaction constant.

$$\Delta = \Delta h - T\Delta s, \tag{2}$$

where Δh and Δs are the enthalpy and entropy costs associated with a spin switch at single non-interacting site, respectively. In the mean field approximation, the single-site Hamiltonian reads:

$$h_0 = \Delta\sigma + J\sigma\langle\sigma\rangle. \tag{3}$$

Here every spin-active molecule is considered as a two-level system and surrounding spin states are replaced by the average value $\langle\sigma\rangle$:

$$\begin{aligned} E_{-1} &= -\Delta - J\langle\sigma\rangle \\ E_{+1} &= \Delta + J\langle\sigma\rangle \end{aligned} \tag{4}$$

More information on the model and its current development can be found in the work by Pavlik & Linares (2018), here we focus on the possible effect of the disorder induced by radiation.

First, we assume that the radiation-induced disorder can be represented by an average value, $\langle S\rangle$ and that its effects can be approximated as an effective mean field:

$$h_1 = \Delta\sigma + J\sigma\langle\sigma\rangle + K\sigma\langle S\rangle, \tag{5}$$

where K is the corresponding effective coupling constant. This assumption implies that (i) radiation damage happens in uncorrelated/non-cooperative fashion, and (ii) the kinetics of spin conversion is much faster than that for the damage. The energy levels are now modified:

$$\begin{aligned} E_{-1} &= -\Delta - J\langle\sigma\rangle - K\langle S\rangle \\ E_{+1} &= \Delta + J\langle\sigma\rangle + K\langle S\rangle. \end{aligned} \tag{6}$$

The expectation value for the spin-state operator is given by

$$\langle\sigma\rangle = \tanh\left(\frac{K\langle S\rangle + J\langle\sigma\rangle - \Delta H + T\Delta S}{T}\right), \tag{7}$$

where $\langle S\rangle$ is an average measure of radiation-induced disorder, it depends on dose, dose rate, temperature, energy of radiation, composition, density and structure of the material, even an approximate form of these dependencies is not known. For the considered case of harvesting the dose on cooling, we simply assume that $\langle S\rangle$ increases while temperature decreases, $\langle S\rangle \approx \alpha(T_{\rm start} - T)$. The numerical solutions of equation (7) are shown in Fig. 5, it is qualitatively mimicking the real scenario. Higher-order polynomial functions for the increase of disorder on cooling might be helpful for a quantitative modelling of the real scenario.

The theoretical approach given above might also be interesting for radiation damage alone and for studying the effect of radiation on various structural processes that are frequently

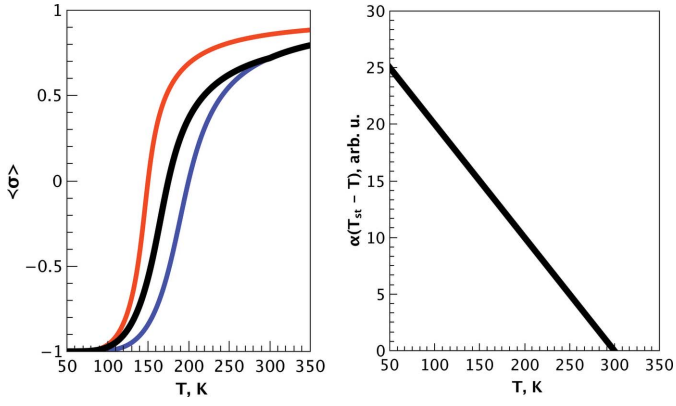

Figure 5
(Left) Expectation value $\langle\sigma\rangle$ as a function of temperature, red curve: ΔH = 400 K, ΔS = 2, no disorder, violet curve: ΔH = 300 K, ΔS = 2, no disorder, black curve: ΔH = 400 K, ΔS = 2, the disorder above $T_{\rm st}$ = 300 K is modelled with α = 0.1, K = 4 K; J = 100 K for all curves. (Right) a measure of radiation-induced disorder as a function of temperature.

modelled with Ising-like models; order–disorder phase transitions, magnetic ordering and gas uptake by porous solids may serve as examples to be tested.

Acknowledgements

The sample used was originally supplied by Dr Paul V. Bernhardt *et al.*, School of Chemistry and Molecular Biosciences, University of Queensland, Brisbane, Australia. The authors also are grateful to the staff of the Swiss–Norwegian BeamLines at the ESRF, Grenoble, France for friendly support, and Dr Chloe Fuller for her help with modeling spin transition curves.

References

Bernhardt, P. V., Bilyj, J. K., Brosius, V., Chernyshov, D., Deeth, R. J., Foscato, M., Jensen, V. R., Mertes, N., Riley, M. J. & Törnroos, K. W. (2018). *Chem. Eur. J.* **24**, 5082–5085..

Bogdanov, N. E., Zakharov, B. A., Chernyshov, D., Pattison, P. & Boldyreva, E. V. (2021). *Acta Cryst.* **77**, 365–370.

Bras, W., Myles, D. A. A. & Felici, R. (2021). *J. Phys. Condens. Matter*, **33**, 423002.

Chernyshov, D., Dyadkin, V. & Törnroos, K. W. (2019). *Acta Cryst.* **75**, 678–678.

Chernyshov, D., Klinduhov, N., Törnroos, K. W., Hostettler, M., Vangdal, B. & Bürgi, H.-B. (2007). *Phys. Rev. B*, **76**, 014406.

Christensen, J., Horton, P. N., Bury, C. S., Dickerson, J. L., Taberman, H., Garman, E. F. & Coles, S. J. (2019). *IUCrJ*, **6**, 703–713.

Coates, C. S., Murray, C. A., Boström, H. L. B., Reynolds, E. M. & Goodwin, A. L. (2021). *Mater. Horiz.* **8**, 1446–1453.

Collet, E. & Guionneau, P. (2018). *C. R. Chim.* **21**, 1133–1151.

Dyadkin, V., Pattison, P., Dmitriev, V. & Chernyshov, D. (2016). *J. Synchrotron Rad.* **23**, 825–829.

Gütlich, P., Ksenofontov, V. & Gaspar, A. B. (2005). *Coord. Chem. Rev.* **249**, 1811–1829.

Kuroda-Sowa, T., Isobe, R., Yamao, N., Fukumasu, T., Okubo, T. & Maekawa, M. (2017). *Polyhedron*, **136**, 74–78.

Lawrence Bright, E., Giacobbe, C. & Wright, J. P. (2021). *J. Synchrotron Rad.* **28**, 1377–1385.

Lemercier, G., Bréfuel, N., Shova, S., Wolny, J. A., Dahan, F., Verelst, M., Paulsen, H., Trautwein, A. X. & Tuchagues, J.-P. (2006). *Chem. Eur. J.* **12**, 7421–7432. .

Murray, K. S. (2013). *The Development of Spin-Crossover Research.* John Wiley and Sons, Ltd.

Ndiaye, M., Belmouri, N. E. I., Linares, J. & Boukheddaden, K. (2021). *Symmetry*, **13**, 828..

Nicolazzi, W. & Bousseksou, A. (2018). *C. R. Chim.* **21**, 1060–1074.

Paulsen, H., Schünemann, V. & Wolny, J. A. (2013). *Eur. J. Inorg. Chem.* **2013**, 628–641.

Pavlik, J. & Linares, J. (2018). *C. R. Chim.* **21**, 1170–1178.

Pillet, S. (2021). *J. Appl. Phys.* **129**, 181101.

Rigaku Oxford Diffraction (2015). *CrysAlis Pro*, Version 1.171.38.41. Rigaku Oxford Diffraction, Yarnton, England.

Sheldrick, G. M. (2015*a*). *Acta Cryst.* A**71**, 3–8.

Sheldrick, G. M. (2015*b*). *Acta Cryst.* C**71**, 3–8.

Vankó, G., Renz, F., Molnár, G., Neisius, T. & Kárpáti, S. (2007). *Angew. Chem. Int. Ed.* **46**, 5306–5309.